JOURNAL OF SOLID STATE CHEMISTRY 108, 275–283 (1994)

Properties of K_2NiF_4-Type Oxides $Sr_2FeO_{\sim 4}$

P. Adler

Max-Planck-Institut für Festkörperforschung, Heisenbergstrasse 1, 70569 Stuttgart, Federal Republic of Germany

Received March 8, 1993; in revised form May 27, 1993; accepted May 28, 1993

Slightly oxygen deficient samples of the K_2NiF_4-type oxide Sr_2FeO_4 with tetravalent iron have been prepared from the metal oxides in flowing O_2 gas atmosphere and investigated by resistivity, magnetic susceptibility, and Mössbauer effect measurements. $Sr_2FeO_{\sim 4}$ is a Mott-type antiferromagnetic semiconductor with a Néel temperature T_N of about 60 K. The Mössbauer spectra above T_N consist of a single Fe^{4+} quadrupole doublet with an isomer shift δ of -0.017 mm sec^{-1}. The Mössbauer spectra of the magnetically ordered phase reveal at least four Fe^{4+} hyperfine sextets which are evidence for local structural distortions associated with the phase transition. A charge disproportionation according to 2 $Fe^{4+} \rightarrow Fe^{3+} + Fe^{5+}$ which was found previously for some semiconducting perovskite-type oxoferrates(IV) was neither observed above nor below T_N. The magnetic hyperfine fields B_{hf} derived from the Mössbauer spectra at 8 K range from 25 to 33 T which suggests a formal d^4 high spin configuration with covalent Fe–O bonding for the tetravalent iron. The properties of Sr_2FeO_4 are compared with literature data of the perovskite $SrFeO_3$ and the K_2NiF_4-type phases $(A, A')_2M_{0.5}Fe_{0.5}O_4$($A$, = Ca, Sr, Ba, A' = La, and M = Mg, Zn, Li).

1. INTRODUCTION

Perovskite-type oxides with formally tetravalent iron have attracted considerable interest because of their remarkable electronic properties (1). The cubic perovskite $SrFeO_3$ is an example for the coexistence of metallic conductivity and antiferromagnetic ordering ($T_N \approx 130$ K) (2). The Mössbauer spectra of stoichiometric $SrFeO_3$ samples which can be prepared under high oxygen pressures (2, 3) or electrochemically (4) show a single line above T_N and a single magnetic hyperfine sextet below T_N in agreement with the cubic structure. Stoichiometric $CaFeO_3$ which was also prepared under high oxygen pressures has a perovskite-type structure too and orders antiferromagnetically below $\approx$120 K (5, 6), however, is a semiconductor. The Mössbauer spectra of $CaFeO_3$ below T_N reveal two distinct hyperfine sextets. From the isomer shifts and hyperfine fields it was concluded that a charge disproportionation of the type 2 $Fe^{4+} \rightarrow Fe^{3+} + Fe^{5+}$ occurs (7).[1] Above T_N a paramagnetic mixed valence state with distinct lines for Fe^{3+} and Fe^{5+} is found. Above 290 K a paramagnetic averaged valence state yielding a single line Mössbauer spectrum only occurs. Investigations on solid solutions $Sr_{1-x}Ca_xFeO_3$ (8) and $Sr_{1-x}La_xFeO_3$ (9) confirmed the idea of a charge disproportionation. In particular a gradual change from the $CaFeO_3$-type to the $SrFeO_3$-type Mössbauer spectra was found for the isovalent substitution of Ca^{2+} by Sr^{2+}. Also oxygen deficient $SrFeO_{3-y}$ samples were studied (3, 10, 11).

Other examples for a charge disproportionation of Fe^{4+} have been reported for the Fe^{4+}/Fe^{3+} mixed valence oxides $Ba_{1-x}La_xFeO_{3-y}$ (12) and $Sr_2LaFe_3O_{8+y}$ (13). In contrast to $CaFeO_3$ a direct transition from a paramagnetic averaged valence phase to an antiferromagnetic mixed valence phase occurs in these oxides. No paramagnetic mixed valence phase was found. The results of a low temperature neutron diffraction study of $Sr_2LaFe_3O_{8.94}$ were interpreted in terms of charge density and spin density waves although surprisingly no periodic structural distortion was observed (14).

Not only the charge disproportionation but also the spin state of Fe^{4+} has been a subject of discussion (15). An Fe^{4+} ion in octahedral coordination environment may have either a ^5E_g ground state arising from the $t_{2g}^3e_g^1$ high spin configuration or a $^3T_{1g}$ ground state arising from the t_{2g}^4 low spin configuration. While the magnetic moment of 1.6 μ_B per Fe^{4+} ion derived from a neutron diffraction study of $SrFeO_{2.9}$ at 77 K was considered as evidence for a low spin configuration of Fe^{4+} (16) the rather large value of 33 T for the internal field obtained from Mössbauer spectra of $SrFeO_3$ is more in favor of a high spin configuration.

Beside the metaferrates $AFeO_3$ (A = Ca, Sr, Ba) also orthoferrates A_2FeO_4 (A = Sr, Ba) (17) and a Ruddlesden-Popper-type phase $Sr_3Fe_2O_7$ (18) with tetravalent iron are known. Mössbauer spectra and a neutron diffraction

[1] Throughout the paper the ionic charge limit is used for the characterization of the different oxidation states of iron. As a result of covalent Fe–O bonding the actual charges may be considerably different.

0022-4596/94 $6.00

study of $Sr_3Fe_2O_{7-y}$ ($0 \leq y \leq 1$) have been reported (19, 20). There is some evidence that also the Mössbauer spectra of $Sr_3Fe_2O_{6.9}$ reflect a $2\ Fe^{4+} \rightarrow Fe^{3+} + Fe^{5+}$ charge disproportionation (7). The only data available concerning the electronic state of iron in the Sr_2FeO_{4-y} system are a few Mössbauer spectra of a strongly oxygen-deficient $Sr_2FeO_{3.7}$ sample which confirmed the existence of Fe^{4+} beside Fe^{3+} (19). A recent structure determination of stoichiometric Sr_2FeO_4 in agreement with previous results revealed that the compound has the K_2NiF_4-type structure (21). Fe^{4+} has also been stabilized in K_2NiF_4-type compounds $(A, A')_2Fe_{0.5}M_{0.5}O_4$ with A = Ca, Sr, Ba, A' = La, and M = Mg, Zn, Li (15, 22, 23). As a consequence of the M^{n+} ions which occupy half of the Fe^{4+} positions in the crystal structure the FeO_6 octahedra are more distorted and more isolated than in the other oxides where the FeO_6 units are linked in two (Sr_2FeO_4) or three ($SrFeO_3$) dimensions. From susceptibility measurements a d^4 high spin configuration was found.

Oxides with K_2NiF_4-type and related structures reveal a rich variety of electrical and magnetic properties (24, 25), especially high temperature superconductivity in doped oxocuprates (26). Therefore a more detailed investigation of the properties of Sr_2FeO_4 should be of interest. The present paper reports the results of a study of nearly stoichiometric $Sr_2FeO_{\sim 4}$ samples by Mössbauer spectroscopy, magnetic susceptibility, and electrical resistivity measurements. The results will be compared with those for other oxoferrates(IV).

2. EXPERIMENTAL

$Sr_2FeO_{\sim 4}$ samples were prepared from stoichiometric mixtures of SrO (Johnson Matthey Alfa Products, stored under Ar) and α-Fe_2O_3 (Merck) in oxygen gas atmosphere at ambient pressure. The powders were carefully mixed in a ball mill and heated for 2 days at 650°C in flowing O_2 gas with intermediate grinding. The raw products were pressed into pellets, heated for at least 16 hr in flowing O_2 gas, and furnace cooled. A second batch of samples was prepared at a temperature of 700°C with a final annealing at 400°C. The first batch of samples is referred to as No. 1, the second batch as No. 2.

The Fe^{4+} content was determined by iodometric titrations employing a similar two-step procedure as has been described for the determination of Cu^{3+} in oxocuprates (27). In a first step Fe^{4+} is reduced to Fe^{3+} by heating the Sr_2FeO_{4-y} sample in 1 M HCl. Subsequently the amount of solid KI required for a 0.7 M solution was added. As a consequence of the reduction of Fe^{3+} to Fe^{2+} iodine is liberated which was titrated with 0.04 M $Na_2S_2O_3$. In the second step the Sr_2FeO_{4-y} sample was added in portions under stirring to a 1 M HCl/0.7 M KI solution. The liberated iodine was titrated as above. In this step Fe^{4+} behaves as a two electron oxidant. Therefore the Fe^{4+} content is obtained from the difference between the two titrations.

All titrations were carried out under flowing Ar. The error in the Fe^{4+} content is estimated as ±5%.

^{57}Fe Mössbauer spectra of powdered $Sr_2FeO_{\sim 4}$ samples were measured in an Oxford flow cryostat with a conventional Mössbauer spectrometer operating in the constant acceleration mode. $^{57}Co/Rh$ was used as the γ-ray source. The velocity scale was calibrated by measuring the hyperfine sextet of a α-iron foil. All isomer shifts are referred to α-iron.

Electrical resistivity measurements were performed on pellets of $Sr_2FeO_{\sim 4}$ according to the four point contact method. The resistivities R and the specific resistivities ρ are of the same order of magnitude. Magnetic susceptibility measurements were performed with a SQUID susceptometer in external fields of 1 T (sample No. 1) or 0.1 T (sample No. 2).

3. RESULTS AND DISCUSSION

3.1. Sample Characterization

Sr_2FeO_4 crystallizes in space group $I4/mmm$. The purity of the substances was checked by comparing experimental and calculated X-ray powder patterns and by Mössbauer spectroscopy. No impurity lines were detected in the X-ray diagrams of sample No. 1, weak impurity lines, which could not be identified, were observed for sample No. 2. The lattice constants were a = 3.863(1) Å, c = 12.406(2) Å for No. 1, and a = 3.860(1) Å, c = 12.398(3) Å for No. 2, respectively. The values are in reasonable agreement with a = 3.864 Å and c = 12.397 Å determined by Dann *et al.* (21). The titrations gave Fe^{4+} contents of 88% for sample No. 1, and 82% for sample No. 2, respectively. The room temperature Mössbauer spectra (c.f. Fig. 3) consist of a quadrupole doublet (see below) with an isomer shift $\delta = -0.017$ mm sec^{-1} which is typical for tetravalent iron. In addition a weak hyperfine sextet with δ = 0.36 mm sec^{-1} and a hyperfine field B_{hf} = 51.8 T, values typical for Fe^{3+} is found. Comparison with literature data (28) suggests that the hyperfine sextet is due to a small quantity of unreacted α-Fe_2O_3. Assuming equal Debye–Waller factors for iron in the two phases one estimates Fe^{3+} contributions to the total iron content of 6% for sample No. 1 and 4% for sample No. 2. If the titration results are corrected for the Fe^{3+} impurity contributions one obtains the compositions $Sr_2FeO_{3.97(3)}$ (sample No. 1), and $Sr_2FeO_{3.93(3)}$ (sample No. 2) for the K_2NiF_4-type phases. The Mössbauer spectra will be discussed in more detail in Section 3.4.

In order to facilitate a complete reaction it would be desirable to heat the initial oxide mixture to higher temperatures. In this case, however, the Ruddlesden-Popper-

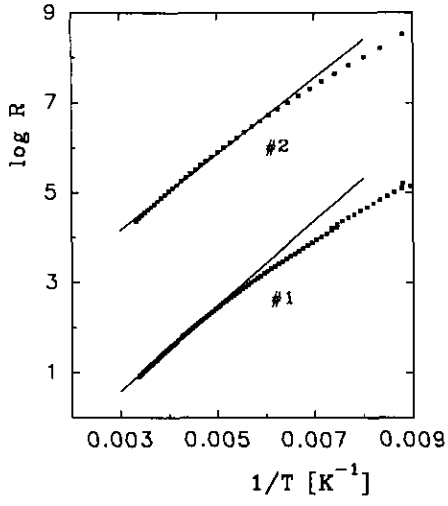

FIG. 1. Resistivity vs inverse temperature for the two samples of $Sr_2FeO_{\sim 4}$.

type phase $Sr_3Fe_2O_{7-y}$ is formed which could only partially be converted into Sr_2FeO_{4-y} by subsequent annealing at lower temperatures at ambient pressure. A complete conversion Sr_2FeO_4 was achieved by annealing under oxygen pressure of 20 MPa (21). The synthesis of stoichiometric Sr_2FeO_4 was reported first by Scholder *et al.* (17) who heated the hydroxo complex $Sr_3[Fe(OH)_6]_2$ with an excess of $Sr(OH)_2$ at 700–800°C in flowing O_2 and removed the excess of $Sr(OH)_2$ with methanol at 0°C.

3.2. Electrical Properties

From the log R (R is the resistivity) vs $1/T$ plot (Fig. 1) it is evident that the $Sr_2FeO_{\sim 4}$ samples are semiconductors. The data deviate from a straight line which is expected if an Arrhenius-type law is assumed for the temperature dependence of the resistivity. This may reflect sample inhomogeneities leading to a distribution of activation energies E_σ for the transport. The absolute values of R were three orders of magnitude larger for the more oxygen deficient sample No. 2 than for sample No. 1, but the curves are essentially parallel.[2] If the data between 150 and 300 K are analyzed by a linear regression one obtains E_σ-values of 0.18 eV for No. 1 and 0.16 eV for No. 2, respectively. The conductivity of the K_2NiF_4-type oxide $Sr_2FeO_{\sim 4}$ is several orders of magnitude lower than that of the perovskite-type oxide $SrFeO_3$ (2). Stoichiometric $SrFeO_3$ is metallic. But also oxygen deficient $SrFeO_{3-y}$ samples with $y = 0.03$ and $y = 0.14$, which are semiconductors, show larger conductivities and smaller activation energies than the $Sr_2FeO_{\sim 4}$ samples.

[2] In the case of sample No. 1 one week after the first measurement the resistivities have increased by two orders of magnitude. This may be indicative of oxygen loss for longer storage times.

3.3. Magnetic Susceptibility Measurements

The magnetic susceptibility curve of $Sr_2FeO_{\sim 4}$ (Fig. 2) reveals a maximum around 60 K. Measurements performed in the zero-field cooled and field cooled mode were in good agreement. The susceptibility data are characteristic for antiferromagnetic ordering with a Néel temperature $T_N \leq 60$ K. Above 60 K the $1/\chi$ vs T plot deviates from a straight line which is expected according to a Curie–Weiss law $\chi = C/(T - \Theta)$. If the temperature range between 200 and 300 K is taken for a linear regression effective moments μ_{eff} of 5.55 μ_B and 5.29 μ_B and paramagnetic Néel temperatures of +50 K and +47 K are obtained for samples No. I and No. 2, respectively. The μ_{eff}-values are larger than the spin-only value of 4.9 μ_B expected for a d^4 high spin configuration. The large μ_{eff}- and positive Θ-values suggest that ferromagnetic interactions are involved in the magnetic structure. The overall phenomenology of the susceptibility data for $Sr_2FeO_{\sim 4}$ is similar as for $SrFeO_3$. Antiferromagnetic ordering occurs around 130 K in the three-dimensional perovskite system. Above T_N μ_{eff}- and Θ-values comparable to the present ones are found if the temperature range between 200 and 300 K is taken for the analysis (2). Susceptibility data of $SrFeO_3$ above 300 K, however, reveal still deviations from linearity in the $1/\chi$ vs T plot (29) which shows that the application of a Curie–Weiss law may not be meaningful. Neutron diffraction measurements on $SrFeO_3$ have been interpreted in terms of a helical spin structure (16, 29). Unlike the results on $SrFeO_3$ and Sr_2FeO_4 the $1/\chi$ vs T plots for substances of the type $(A, A')_2M_{0.5}Fe_{0.5}O_4$ where more isolated Fe^{4+} ions occur are linear between

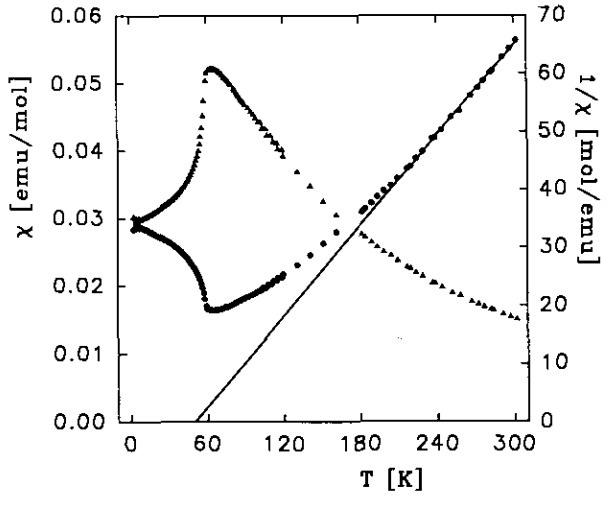

FIG. 2. Temperature dependence of the molar susceptibility χ (left scale) and inverse molar susceptibility $1/\chi$ (right scale) for No. 1. For conversion to SI units (m^3 $mole^{-1}$) the χ-values have to be multiplied with $4\pi \cdot 10^{-6}$.

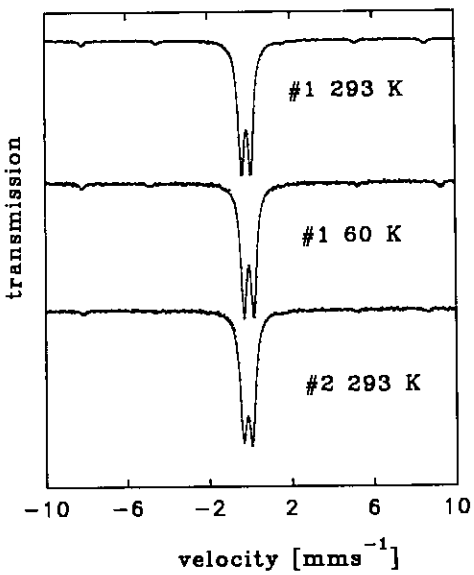

FIG. 3. Mössbauer spectra of the paramagnetic phase of $Sr_2FeO_{\sim 4}$. Transmission ranges are 100–75% and 100–80% for the spectra of No. 1 and No. 2, respectively.

30 and 300 K and μ_{eff}-values close to the spin-only limit of a d^4 high spin configuration were found (15, 22, 23).

3.4. *Mössbauer Spectroscopy*

Mössbauer spectra for the $Sr_2FeO_{\sim 4}$ samples collected at different temperatures are shown in Figs. 3–5. Beside a small fraction of a Fe^{3+} sextet which can be attributed to unreacted α-Fe_2O_3 the spectra between 60 and 290 K consist of two lines. Below 60 K a complicated magnetic hyperfine pattern is found which in agreement with the susceptibility data evidences magnetic ordering. In principal the two lines in the spectra above T_N can either be the components of a quadrupole doublet arising from a single Fe^{4+} species or, similar as for $CaFeO_3$ (7), they can be due to different sites arising from a $2\ Fe^{4+} \rightarrow Fe^{3+} + Fe^{5+}$ charge disproportionation. The latter situation corresponds to isomer shifts $\delta = -0.24$ mm sec^{-1} for the Fe^{5+} and $\delta = 0.20$ mm sec^{-1} for the Fe^{3+} component at 290 K. These values are not within the range of isomer shifts reported so far for the case of charge disproportionation. Furthermore Sr_2FeO_4 crystallizes in the tetragonal space group $I4/mmm$ where the Fe^{4+} site has D_{4h} symmetry. Accordingly a nonzero electric field gradient (efg) is expected and the spectra above T_N are reasonably interpreted in terms of a quadrupole doublet. The quadrupole splitting ΔE_Q does not change much between 60 and 290 K (cf. Table 1). Considering the nearly regular FeO_6 octahedra (bond distances: 4 × 1.932 Å, 2 × 1.950 Å (21)) the splittings of the t_{2g} and e_g orbitals are expected to be small. The quadrupole splitting is rather due to a lattice contribution to the efg tensor than to a valence contribution. In the case of a valence contribution arising either from a $e_g^2 b_{2g}^1 a_{1g}^1$ high spin or from a $e_g^3 b_{2g}^1$ low spin configuration of Fe^{4+} in D_{4h} symmetry (for an elongated octahedron) the quadrupole splitting should be more temperature dependent. The isomer shift is within the range of values typical for Fe^{4+}. The spectra above T_N do not show further Fe^{3+} components but a certain amount of Fe^{3+} may be involved in valence fluctuations which are rapid within the Mössbauer time scale. This may be the reason for the slightly different room temperature Mössbauer parameters of samples No. 1 and No. 2.

From the spectra well below T_N (Fig. 4) it is seen that different Fe^{4+} sites are present in the magnetically ordered phase. In spite of the difficulties to evaluate the complicated spectra quantitatively it is evident that no $2\ Fe^{4+} \rightarrow Fe^{3+} + Fe^{5+}$ charge disproportionation occurs. Beside the Fe^{3+} impurity no additional Fe^{3+} component is found in the spectra of sample No. 1 within the limits of experimental error (≈2%). This suggests that sample No. 1 can be considered as nearly stoichiometric Sr_2FeO_4. A small amount of additional Fe^{3+} (total area fraction ≈3%) which is distributed over at least two sites is found in the 12 K spectrum of sample No. 2. It arises presumably from a small oxygen deficiency. The Fe^{4+} fractions determined from Mössbauer spectroscopy are slightly larger

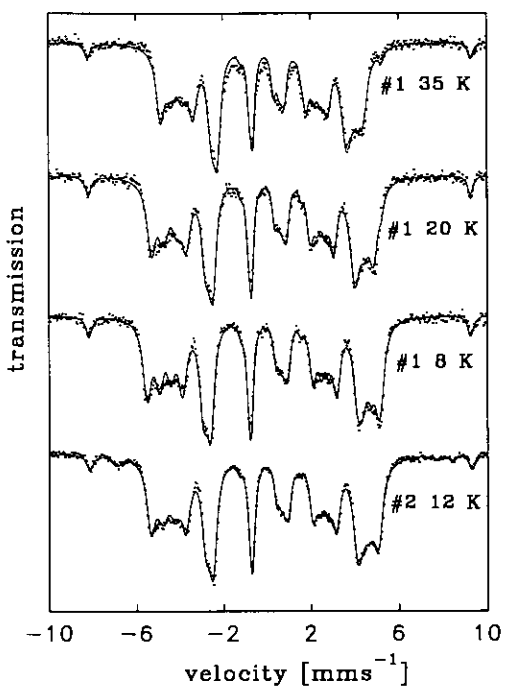

FIG. 4. Mössbauer spectra of the magnetically ordered phase of $Sr_2FeO_{\sim 4}$. Solid lines correspond to the optimal fits to the spectra obtained from the model described in the text. Transmission ranges are 100–92%, and 100–95% for the spectra of No. 1 and No. 2, respectively.

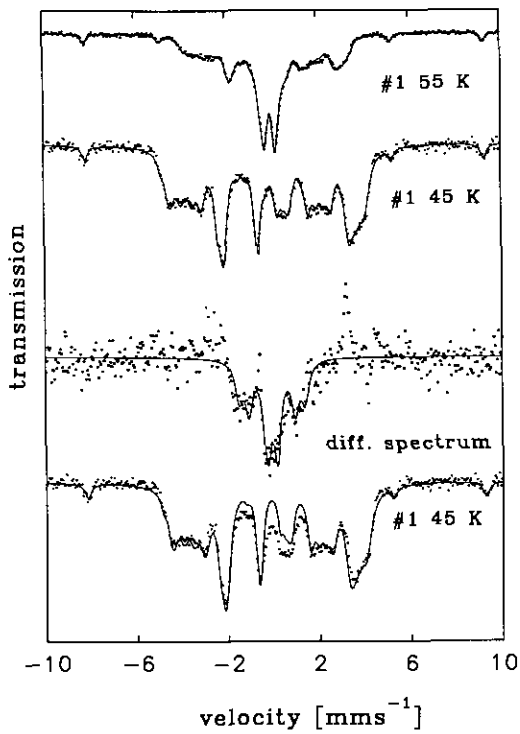

FIG. 5. Mössbauer spectra of $Sr_2FeO_{\sim 4}$ in the temperature range of the antiferromagnetic $\rightleftharpoons$ paramagnetic phase transition. In the lower part of the figure the experimental 45 K spectrum together with the best fit obtained without considering paramagnetic species is shown. Above the difference spectrum is depicted. In the upper part the 45 K and 55 K spectra are shown where the optimal fits include four Fe^{4+} hyperfine sextets and three doublets, respectively. Transmission ranges are 100–92% for the 45 K, and 100–87% for the 55 K spectrum.

than those determined from the chemical analysis, in particular for sample No. 2. A possible origin for this discrepancy may be a certain underestimation of the Fe^{4+} content due to Cl_2 or O_2 gas evolution in the chemical analysis which was performed in an open system or a loss of oxidative power during the storage time of the samples before the analysis was performed. An overestimation of the Fe^{4+} content from the Mössbauer spectra results if the Debye–Waller factor for Fe^{4+} is larger than for Fe^{3+}.

TABLE I
Mössbauer Parameters for the Paramagnetic Phase of $Sr_2FeO_{\sim 4}$

T (K)	δ	ΔE_Q	$\Gamma_{1/2}$
293, No. 1	−0.017(1)	0.452(1)	0.169(1)
293, No. 2	−0.012(1)	0.425(2)	0.186(2)
100, No. 1	0.065(1)	0.474(2)	0.167(1)
60, No. 1	0.069(1)	0.479(2)	0.169(1)

Note. The units are mm sec^{-1}.

The results from chemical analysis, however, require that the f-factor of Fe^{4+} should be more than twice as large as the f-factor of Fe^{3+} which does not seem reasonable. Another possibility is that a small amount of Fe^{3+} is involved in rapid valence fluctuations even at low temperatures.

In order to determine the hyperfine interaction parameters the spectra of sample No. 1 were analyzed by five sextets, four for the Fe^{4+} sites and one for the Fe^{3+} impurity component. Two further Fe^{3+} sextets were added for the reproduction of the 12 K spectrum of sample No. 2. The analysis of the spectra is based on the assumption that the quadrupole interaction is small in comparison with the nuclear Zeeman effect. The theoretical intensity ratios 3 : 2 : 1 : 1 : 2 : 3 which are strictly valid in the limit of thin absorbers were used. Only one linewidth parameter was adjusted. From the spectra at 8 or 12 K identical isomer shifts were obtained for the different Fe^{4+} sites. The δ-values are the same as in the paramagnetic phase at 60 K and were subsequently fixed for the evaluation of the spectra at higher temperatures. The quadrupole splitting parameters ε cannot be simply interpreted because they depend on the relative orientations of the efg tensors with respect to the directions of the hyperfine fields (30). The results of the calculations are summarized in Table 2. From Fig. 4, it is seen that the main structures of the spectra well below T_N (8–35 K) are reasonably reproduced by the model. The remaining deviations between theoretical and experimental spectra, namely the line broadenings in the experimental spectra, indicate that the actual distribution of hyperfine fields is more complex. Furthermore, polarization effects due to the finite absorber thickness may cause deviations from the theoretical intensity ratios. Also the line positions of the 45 K spectrum (Fig. 5) are reasonably reproduced but a significant deviation between theoretical and experimental spectra is found in the vicinity of $v = 0$ mm sec^{-1}. From the difference spectrum between experimental and theoretical data it is seen that part of the deviation is due to the presence of a certain amount of paramagnetic Fe^{4+} phase which contributes a quadrupole doublet with $\Delta E_Q = 0.46$ mm sec^{-1} as in the spectra of the pure paramagnetic phase. But even after subtraction of this component an additional broadened doublet structure centered around 0.07 mm sec^{-1} with a large splitting of ca. 2.4 mm sec^{-1} remains. The statistics of the difference spectrum is not sufficient to decide safely whether the feature arises from collapsing magnetic hyperfine patterns or from additional quadrupole doublets corresponding to intermediate paramagnetic Fe^{4+} species with distorted coordination geometry. If the difference spectrum is approximated by three doublets a reasonable fit of the total 45 K spectrum is achieved (Fig. 5). The 55 K spectrum clearly reveals the coexistence of paramagnetic and magnetically ordered

TABLE II
Mössbauer Parameters for the Magnetically Ordered Phase of $Sr_2FeO_{\sim 4}$

	T (K) →	8[a]	12[b]	20[a]	35[a]	45[a]	55[a]
Fe(m1)	δ	0.071(6)	0.074(4)	0.07*	0.07*	0.07*	0.07*
	ε	−0.155(5)	−0.148(5)	−0.158	−0.168	−0.155*	−0.155*
	B_{hf}	32.80(6)	32.05(3)	31.37(6)	28.54(9)	26.43(6)	22.15(15)
	area (%)	30.4(10)	30.1(7)	32.1(10)	28.3(15)	25.5(11)	12.0(12)
Fe(m2)	δ	0.067(10)	0.084(8)	0.07*	0.07*	0.07*	0.07*
	ε	−0.070(10)	−0.058(8)	−0.065(10)	−0.083(10)	−0.075*	−0.075*
	B_{hf}	30.03(12)	29.03(9)	28.20(12)	26.12(15)	23.85(12)	20.13(15)
	area (%)	18.0(12)	18.7(9)	19.4(12)	19.1(16)	19.0(14)	14.0(14)
Fe(m3)	δ	0.070(10)	0.065(7)	0.07*	0.07*	0.07*	0.07*
	ε	0.020(10)	0.022(8)	0.020(15)	−0.010(13)	0.02*	0.02*
	B_{hf}	27.15(9)	26.26(9)	25.34(15)	23.57(15)	21.46(12)	17.77(12)
	area (%)	19.0(11)	17.4(10)	16.4(15)	17.9(16)	18.9(14)	16.3(12)
Fe(m4)	δ	0.068(7)	0.071(5)	0.07*	0.07*	0.07*	0.07*
	ε	0.178(8)	0.178(5)	0.188(10)	0.170(8)	0.178*	0.178*
	B_{hf}	24.75(6)	24.19(6)	23.73(9)	21.52(6)	19.82(9)	15.84(12)
	area (%)	26.7(10)	26.4(8)	26.8(14)	30.2(12)	22.2(11)	11.2(10)
Fe(d1)	δ					0.07*	0.078(2)
	ΔE_Q					0.46(3)	0.465(4)
	area (%)					5.6(3)	31.8(4)
Fe(d2)	δ					0.07*	0.07*
	ΔE_Q					2.02(11)	1.63(3)
	area (%)					2.7(4)	6.6(3)
Fe(d3)	ε					0.07*	0.07*
	ΔE_Q					2.89(14)	2.65(4)
	area (%)					1.7(2)	2.6(2)

Note. The notation mi, i = 1, 2, 3, 4 refers to magnetic sextets, the notation di, i = 1, 2, 3 to doublets. The difference of the area fractions to 100% corresponds to the Fe^{3+} components. The full linewidths at half height Γ are in the range 0.30–0.60 mm sec^{-1}. The units are mm sec^{-1} for δ, ε, ΔE_Q, and Tesla for B_{hf}.

[a] Sample No. 1.

[b] Sample No. 2.

* Parameter not varied.

phase. Again a reasonable fit of the spectrum with fixed ε-parameters and a consistent temperature dependence of the hyperfine fields is obtained if in addition to the obvious paramagnetic Fe^{4+} site two further doublets are included in the evaluation. A detailed inspection of the 35 K spectrum also reveals some deviations between the theoretical and experimental spectrum near v = 0 mm sec^{-1}. Thus it is concluded that the transition to the paramagnetic phase begins already around ca. 35 K.

From the Mössbauer spectra it is clear that all iron atoms in the stoichiometric compound Sr_2FeO_4 are in the valence state +4. A Fe^{3+}/Fe^{5+} mixed valence phase which was observed for some oxoferrates(IV), is found neither in the paramagnetic nor in the antiferromagnetic phase. The isomer shift of Fe^{4+} in Sr_2FeO_4 is intermediate within the range of values found previously (cf. Table 3). On the basis of recent photoemission experiments on $SrFeO_3$ (31) it was suggested that the ground state ψ_g of Fe^{4+} can be described by a cluster configuration interaction model as

$$\psi_g = a\,|\,d^4> + b\,|\,d^5L^{-1}>, \qquad (1)$$

where $|d^4>$ corresponds to the ionic limit and $|d^5L^{-1}>$ to O $2p \rightarrow$ Fe $3d$ charge transfer configurations. It is expected that the weight of the d^5L^{-1} configurations increases from the more isolated Fe^{4+} ions found in the compounds $(A, A')_2M_{0.5}Fe_{0.5}O_4$ via the two-dimensional Fe–O network of Sr_2FeO_4 to the three-dimensional Fe–O network of $SrFeO_3$. Accordingly the shielding of the s electron density from the iron nucleus becomes stronger

TABLE 3
Comparison of Isomer Shifts and Hyperfine Fields of Some Oxoferrates(IV)

	Sr_2FeO_4	$SrFeO_3$	$(A, A')_2M_{0.5}Fe_{0.5}O_4$	$CaFeO_3$
δ (mm sec^{-1})	−0.017 (293 K) 0.07 (8 K)	0.054 (300 K) 0.146 (4 K)	−0.20– −0.14 (300 K) −0.13– −0.06 (4 K)	0.073 (300 K)[a] 0.34 (Fe^{3+}, 4 K) 0.00 (Fe^{5+}, 4 K)
B_{hf} (T)	24.8–32.8	33.1	13–18	41.6 (Fe^{3+}) 27.9 (Fe^{5+})
Ref.	this work	(3)	(15, 22, 23)	(7)

[a] Average valence phase.

and leads to more positive δ-values. From Fe $2p$ photoelectron spectra of $SrFeO_3$ it was concluded that ψ_g is strongly hybridized according to Eq. (1) with a dominant d^5L^{-1} contribution (31).

From the complicated Mössbauer spectra below T_N it is concluded that the transition from the paramagnetic to the antiferromagnetic phase is accompanied by local structural rearrangements which give rise to several different Fe^{4+} sites in the antiferromagnetic phase. Above T_N only one Fe^{4+} site yielding a sharp quadrupole doublet is found, in agreement with the expectations from the room temperature crystal structure. The magnetic hyperfine fields at the Fe^{4+} sites of Sr_2FeO_4 at 8 K which are expected to be close to the saturation values range from 25 to 33 T. The maximum value is nearly the same as in the antiferromagnetic phase of $SrFeO_3$. In general B_{hf} is a sum of three contributions: (32)

$$B_{hf} = B_c + B_L + B_D. \tag{2}$$

B_c is the Fermi contact contribution arising from the polarization of the s electrons by the partially filled $3d$ shell, B_L is a contribution due to the angular momentum of the electronic shell, and B_D is due to the dipole–dipole interaction between the electronic spin and the magnetic moment of the nucleus. B_c is determined by the number of unpaired electrons. If the magnitude of B_c is approximated as 22 $\langle S_z \rangle$ Tesla (32), B_c is estimated as 44 T for a d^4 high spin and as 22 T for a d^4 low spin configuration. These values are expected to be considerably reduced by the covalency of the Fe–O bonding in oxoferrates(IV). Fe^{4+} has cubic site symmetry in the crystal structure of $SrFeO_3$. In this case B_D and for a d^4 high spin configuration also B_L, which is proportional to the expectation value $\langle L \rangle$ of the angular momentum, vanish. Thus B_{hf} = 33 T is interpreted as the Fermi contact field B_c of covalently bound Fe^{4+} high spin. The spin state of Fe^{4+} has been the subject of controversal discussions. Beside the Mössbauer spectra also cluster model calculations and Fe $3s$ photoelectron spectra support a strongly covalent $t_{2g}^3e_g^1$ high spin configuration of Fe^{4+} in $SrFeO_3$ (31, 33). The similar B_{hf}-values as well as the similar magnetic behavior of $SrFeO_3$ and Sr_2FeO_4 evidence that the spin state of Fe^{4+} is the same for the two compounds; i.e., Fe^{4+} has a formal d^4 high spin configuration in Sr_2FeO_4. The Fe^{4+} sites with lower B_{hf}-values presumably correspond to more distorted sites. It is noted in this context that small B_{hf}-values of 12–18 T were derived for the d^4 high spin compounds $(A, A')_2M_{0.5}Fe_{0.5}O_4$ (15, 22, 23) where elongated FeO_6 octahedra occur. In this case B_D and, depending on the actual point symmetry of Fe^{4+} in the magnetically ordered phase, also B_L may contribute to B_{hf} and compensate B_c.

The temperature dependence of B_{hf} reflects the temperature dependence of the magnetization M when B_{hf} is mainly determined by B_c. B_c as well as M are proportional to the expectation value $\langle S \rangle$ of the electronic spin. The reduced hyperfine fields $b(T) = B_{hf}(T)/B_{hf}^0$ with $B_{hf}^0 \approx B_{hf}$ (8 K) show that the degree of magnetization is the same for the different Fe^{4+} sites in the magnetically ordered phase of Sr_2FeO_4. The temperature dependence of b was reproduced by

$$b(T) = B^*(1 - T/T_N)^{\beta^*}. \tag{3}$$

From the Mössbauer spectra it is seen that the magnetic ordering vanishes completely within the range 55 K < T_N < 60 K. Choosing T_N = 60 K as an upper limit one obtains from a fit of Eq. (3) to the experimental data a mean value of β^* = 0.18(1), and B^* = 1.02(1). The result for β^* is an upper limit as β^* becomes smaller if smaller T_N-values are chosen. The experimental data for B_{hf} are depicted together with the curves calculated from Eq. (3) in Fig. 6. Similar β^*-values have been reported for other antiferromagnetic quasi-2-D layer compounds as e.g. K_2NiF_4 (β^* = 0.14), K_2MnF_4 (β^* = 0.15) etc. (34). In

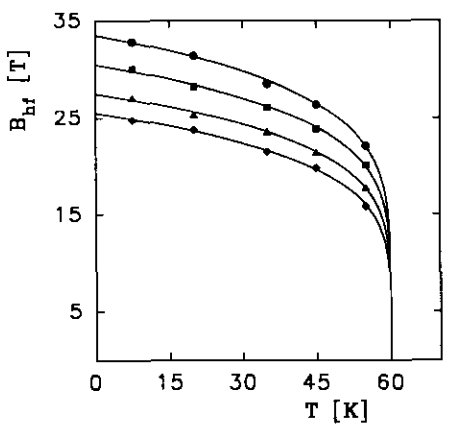

FIG. 6. Temperature dependence of the magnetic hyperfine fields for the different Fe^{4+} sites in the magnetically ordered phase of $Sr_2FeO_{\sim 4}$. The solid lines correspond to a fit of the experimental data to Eq. (3).

the vicinity of the critical region, i.e. for small values of $t = 1 - T/T_N$, Eq. (3) defines the critical exponent β ($\beta = \lim_{t\to 0} \beta^*$) for the phase transition. The β^*-values for Sr_2FeO_4 and related compounds correspond roughly to the theoretical limit of $\beta = \frac{1}{8}$ for two-dimensional magnetic ordering. For three-dimensional ordering $\beta \approx \frac{1}{3}$ is predicted. Reliable experimental values for β, however, require the analysis of data with $t < 10^{-2}$ (35) which are not available for Sr_2FeO_4. Furthermore the coexistence of paramagnetic and antiferromagnetic phase seen in the 45 and 55 K Mössbauer spectra suggests rather a distribution of Néel temperatures than a definite T_N. Probably the mechanism of the antiferromagnetic $\rightleftharpoons$ paramagnetic transition is not only determined by the spin interactions but also by structural reorganizations which lead to distinguishable Fe^{4+} sites in the magnetically ordered phase. The driving force for these distortions may be a Jahn–Teller instability of the ^5E_g (O_h) high spin state which has been established for the isoelectronic Mn^{3+} ion (36). It has been suggested that the Jahn–Teller instability is suppressed in $SrFeO_3$ because of the itinerant nature of the valence electrons (7). Also the nearly regular FeO_6 coordination geometry in Sr_2FeO_4 at room temperature is not in favor of a Jahn–Teller effect. As is apparent from the resistivity measurements, however, the itineracy of the valence electrons of $Sr_2FeO_{\sim 4}$ is strongly reduced, in particular at low temperatures. Accordingly the Jahn–Teller instability for Fe^{4+} may be suppressed in the antiferromagnetic, metallic phase of $SrFeO_3$, but lead to distorted Fe^{4+} sites in the antiferromagnetic, insulating phase of $Sr_2FeO_{\sim 4}$. The Fe^{3+} oxides $SrLnFeO_4$ (Ln = La, Pr, Nd, Eu, Gd) do not show comparable distortions in the magnetically ordered phase (37, 38). For some of the compounds, however, spin reorientation processes were found.

4. CONCLUSIONS

The present resistivity, susceptibility, and Mössbauer effect investigations on nearly stoichiometric samples $Sr_2FeO_{\sim 4}$ demonstrate that Sr_2FeO_4 is an antiferromagnetic semiconductor. Local magnetic moments occur above and below T_N. Thus Sr_2FeO_4 as many other transition metal oxides has to be considered as a Mott-type insulator. In agreement with the general trends found when K_2NiF_4-type phases are compared with the corresponding perovskite-type phases the conductivity and the magnetic ordering temperature for Sr_2FeO_4 are smaller than for $SrFeO_3$. This corresponds to the fact that the Fe–O–Fe interactions are restricted to two dimensions in Sr_2FeO_4 but become three-dimensional in $SrFeO_3$. For the same reason the Mössbauer isomer shift of Fe^{4+} is more negative for Sr_2FeO_4 than for $SrFeO_3$. Neither $SrFeO_3$ nor Sr_2FeO_4 show a $2\,Fe^{4+} \rightarrow Fe^{3+} + Fe^{5+}$ charge disproportionation. In contrast to $SrFeO_3$ where the Mössbauer spectra of the antiferromagnetic phase reveal a single Fe^{4+} site the paramagnetic $\rightarrow$ antiferromagnetic phase transition of Sr_2FeO_4 is accompanied by local structural distortions resulting in different Fe^{4+} sites below T_N. The latter may be a consequence of a Jahn–Teller instability of the ^5E_g high spin state. Low temperature neutron diffraction studies are required to decide whether the structural distortions are periodically ordered. Also a determination of the magnetic structure would be interesting. The complicated Mössbauer spectra below T_N, and the deviation from linearity in the $1/\chi$ vs T plot with positive Θ- and large μ_{eff}-values suggest a complex magnetic behavior involving ferromagnetic interactions. Further studies on Sr_2FeO_4 with cationic substitutions are in progress to investigate the electronic structure and chemical bonding of Fe^{4+} within the K_2NiF_4-type structure.

ACKNOWLEDGMENTS

I wish to express my sincere thanks to Professor P. Gütlich, University of Mainz (FRG), for the possibility to perform the Mössbauer experiments in his laboratory. I thank Dr. U. Stumm, Dr. H. Spiering, and in particular Dr. J. Ensling for experimental help and helpful discussions. Furthermore I thank N. Weishaupt for the resistivity, E. Brücher for the magnetic susceptibility measurements, and Professor A. Simon for his support of this work. I am indebted to Dr. R. K. Kremer for critical reading of the manuscript.

REFERENCES

1. Review; M. Takano and Y. Takeda, *Bull. Inst. Chem. Res. Kyoto Univ.* **61,** 406 (1983).
2. J. B. MacChesney, R. C. Sherwood, and J. F. Potter, *J. Chem. Phys.* **43,** 1907 (1965).
3. P. K. Gallagher, J. B. MacChesney, and D. N. E. Buchanan, *J. Chem. Phys.* **41,** 2429 (1964).
4. A. Wattiaux, L. Fournes, A. Demourgues, N. Bernaben, J. C. Grenier, and M. Pouchard, *Solid State Commun.* **77,** 489 (1991).
5. F. Kanamaru, H. Miyamoto, Y. Mimura, M. Koizumi, M. Shimada, S. Kume, and S. Shin, *Mater. Res. Bull.* **5,** 257 (1970).
6. Y. Takeda, S. Naka, M. Takano, T. Shinjo, T. Takada, and M. Shimada, *Mater. Res. Bull.* **13,** 61 (1978).
7. M. Takano, N. Nakanishi, Y. Takeda, S. Naka, and T. Takada, *Mater. Res. Bull.* **12,** 923 (1977).
8. Y. Takeda, S. Naka, and M. Takano, *J. Phys. Colloq.* **40,** C2-331 (1979).
9. M. Takano, J. Kawachi, N. Nakanishi, and Y. Takeda, *J. Solid State Chem.* **39,** 75 (1981).
10. M. Takano, T. Okita, N. Nakayama, Y. Bando, Y. Takeda, O. Yamamoto, and J. B. Goodenough, *J. Solid State Chem.* **73,** 140 (1988).
11. T. C. Gibb, *J. Chem. Soc. Dalton Trans.*, 1455 (1985).
12. T. C. Gibb and M. Matsuo, *J. Solid State Chem.* **81,** 83 (1989).
13. P. D. Battle, T. C. Gibb, and S. Nixon, *J. Solid State Chem.* **77,** 124 (1988).
14. P. D. Battle, T. C. Gibb, and P. Lightfoot, *J. Solid State Chem.* **84,** 271 (1990).
15. G. Demazeau, Z. Li-Ming, L. Fournes, M. Pouchard, and P. Hagenmuller, *J. Solid State Chem.* **72,** 31 (1988).

16. H. Oda, Y. Yamaguchi, H. Takei, and H. Watanabe, *J. Phys. Soc. Jpn.* **42,** 101 (1977).
17. R. Scholder, H. v. Bunsen, and W. Zeiss, *Z. Anorg. Allg. Chem.* **283,** 330 (1956).
18. C. Brissi, *Ann. Chim. Rome* **51,** 1399 (1961).
19. P. K. Gallagher, J. B. MacChesney, and D. N. E. Buchanan, *J. Chem. Phys.* **45,** 2466 (1966).
20. S. E. Dann, M. T. Weller, and D. B. Currie, *J. Solid State Chem.* **97,** 179 (1992).
21. S. E. Dann, M. T. Weller, and D. B. Currie, *J. Solid State Chem.* **92,** 237 (1991).
22. G. Demazeau, N. Chevreau, L. Fournes, J.-L. Soubeyroux, Y. Takeda, M. Thomas, and M. Pouchard, *Rev. Chim. Miner.* **20,** 155 (1983).
23. L. Fournes, G. Demazeau, Z. Li-Ming, N. Chevreau, and M. Pouchard, *Hyperfine Intact.* **53,** 335 (1990).
24. P. Ganguly and C. N. R. Rao, *J. Solid State Chem.* **53,** 193 (1984).
25. C. N. R. Rao, P. Ganguly, K. K. Singh, and R. A. Mohan Ram, *J. Solid State Chem.* **72,** 14 (1988).
26. J. G. Bednorz and K. A. Müller, *Z. Phys. B: Condens. Matter* **64,** 189 (1986).
27. D. C. Harris and T. A. Hewston, *J. Solid State Chem.* **69,** 182 (1987).
28. O. C. Kistner and A. W. Sunyar, *Phys. Rev. Lett.* **4,** 412 (1960).
29. T. Takeda, Y. Yamaguchi, and H. Watanabe, *J. Phys. Soc. Jpn.* **33,** 967 (1972).
30. G. Le Caër, J.-M. Dubois, L. Häggström, and T. Ericsson, *Nucl. Instr. Meth.* **157,** 127 (1978).
31. A. E. Bocquet, A. Fujimori, T. Mizokawa, T. Saitoh, H. Namatame, S. Suga, N. Kimizuka, Y. Takeda, and M. Takano, *Phys. Rev. B* **45,** 1561 (1992).
32. N. N. Greenwood and T. C. Gibb, "Mössbauer Spectroscopy," p. 60. Chapman and Hall, London, (1971).
33. H. Adachi and M. Takano, *J. Solid State Chem.* **93,** 556 (1991).
34. R. J. Birgeneau, J. Als-Nielsen, and G. Shirane, *Phys. Rev. B* **16,** 280 (1977).
35. H. Keller and I. M. Savić, *Phys. Rev. B* **28,** 2638 (1983).
36. P. Köhler, W. Massa, D. Reinen, B. Hofmann, and R. Hoppe, *Z. Anorg. Allg. Chem.* **446,** 131 (1978).
37. M. Shimada, M. Koizumi, M. Takano, T. Shinjo, and T. Takada, *J. Phys. Colloq.* **40,** C2-272 (1979).
38. D. Hanžel, *J. Phys. Colloq.* **41,** C1-159 (1980).